



Evaluation of laser cleaning effect for the removal of paint on aluminum alloys

Zejia Zhao^{1,2} · Xin Liu^{1,2} · Ziyu Chen³ · Ye Tian^{1,2} · Mingjun Chen^{1,2} · Lisa Liu^{1,2} · Feng Song^{1,2}

Received: 23 September 2022 / Accepted: 4 March 2023 / Published online: 29 March 2023
© The Author(s), under exclusive licence to Springer-Verlag London Ltd., part of Springer Nature 2023

Abstract

The removal of paint as an industrial requirement is still a significant issue in the fields of ship and aircraft skins. How to judge the effect of laser cleaning after the removal of paint on the substrate is a tough problem. The effect is evaluated primarily by considering the amount of paint residue and the extent of substrate surface damage. The amount of paint residue is analyzed by field emission scanning electron microscopy (FE-SEM), energy-dispersive spectroscopy (EDS), Fourier-transform infrared spectrum (FTIR), and photothermal conversion performance. The damage to the substrate surface is assessed utilizing an X-ray diffractometer (XRD) and true color confocal microscope (TCCM). The results manifest that the paint can be completely removed at a laser energy density of 1.66 J/cm². When laser energy density is 1.78 J/cm², the surface of Al alloy appears some nanostructures. This work offers fundamental research and practical guidance for laser cleaning of paint on an aluminum alloy surface.

Keywords Laser cleaning · Paint · The effect · Thermal decomposition · Nanostructures

1 Introduction

Aluminum (Al) alloy, because of its excellent properties including high strength, good toughness, and corrosion resistance, is playing an important role in various fields such as high-speed rail, ship, spacecraft, and aircraft [1–3]. Al alloy is commonly designed in the manufacture of these facilities' skin. Lifetime service for Al alloy can make these properties decline [4]. To prolong the lifetime, paint is always coated on the surface of Al alloy. Many practical results manifest that Al alloy coating used for disparate working environments performs serious durability problems because of the inherent structural features giving rise to damage in various ways, such as aging, cracking, functional failure, and shedding [5, 6]. Just because of this, it is necessary to remove periodically paint coating after applying Al

alloy paint coating as facilities skin for some time. There have been several methods to remove paint on the surface of Al alloy, such as mechanical cleaning, chemical solvent cleaning, water-jet assisted cleaning, and ultrasonic cleaning technologies [7–9]. Although great breakthroughs have been made in removal methods of paint in the past years, some drawbacks are remained to be solved including environmental pollution, low efficiency, secondary damage, and poor surface integrity.

Recently, non-contact laser cleaning with the advantages of being environmentally friendly and high cleaning precision and efficiency has been considered to be a promising laser material treatment technology for achieving high-quality and non-destructive removal of paint [10, 11]. The preliminary investigation on the interaction between laser irradiation and paint derives from the 1990s. Tsunemi et al. confirmed the removal of a paint film thickness of 80 μm from the Al substrate surface by CO₂ pulse laser irradiation in a short time [12]. As a result, through the optimization of laser parameters and repeated laser irradiation, excellent removal characteristics were obtained. The laser cleaning process depends on many factors. The laser source (e.g., output power, wavelength, and pulse duration) plays a significant role in the laser cleaning. The high photon energy of UV laser leads to direct intermolecular bond breaking of

✉ Feng Song
fsong@nankai.edu.cn

¹ School of Physics & The Key Laboratory of Weak Light Nonlinear Photonics, Ministry of Education, Nankai University, Tianjin 300071, China

² Collaborative Innovation Center of Extreme Optics, Shanxi University, Taiyuan 030006, Shanxi, China

³ Huzhou College, Huzhou, China

paint [13]. However, due to some disadvantages of low efficiency and high cost, UV laser is seldom used in industrial cleaning applications [14]. The nanosecond Nd:YAG laser, due to its outstanding characteristic of short pulse duration, limited expansion of heat-affected zone, and higher peak power, has become the mainstream equipment in this field. An increasing number of researchers investigate the removal of paint using a nanosecond Nd:YAG laser based on a combination of experiment and theory [15, 16]. Song et al. utilized Q-switched Nd:YAG laser with the wavelength of 1064 nm to remove paint from the iron substrate, and the results showed that single-pass laser irradiation gave rise to complete paint removal and low-damage substrate in the two-layer coating–substrate system [17]. To achieve accurate paint stripping, Han et al. numerically evaluated the spatial distribution of the temperature as well as thermal stress in terms of the thermodynamic equations, providing curves of paint thickness versus threshold fluences as the reference standard of laser parameter selection [18]. Lu et al. developed a 2D finite-element model to describe in detail physical and chemical processes. The paint removal mechanisms were thermal ablation and vibration effect [19]. Zhao et al. selected the appropriate combination of the overlap amount between laser spots and other laser parameters to improve the removal effect of paint [20]. Despite the thriving research on laser cleaning of paint, the evaluation of the laser cleaning effect of paint from the surface of Al alloy is rarely reported in the field of laser cleaning. For laser cleaning of paint on Al alloy substrate surface, it is well known that there are two possible emergent outcomes which are paint residue and substrate surface damage, respectively. As an important consideration, the suitable evaluation approaches of laser cleaning effect are equally crucial for beneficial properties' performance in the fields of facilities skin. In addition, the laser energy density is sufficient to make substrate surface damage. The high energy can lead to the formation of nanostructures on the surface of the substrate. However, there is a lack of observation and analysis of the nanostructures. Whether laser cleaning as a paint removal technology can achieve surface nanofabrication is worth discussing. Thus, it is essential to further explore this content.

The main work of the study is to discuss the effect of different laser energy densities on the removal of paint on the surface of Al alloy. In this work, we emphatically analyze how to judge the effect of laser cleaning after the removal of paint on the substrate. Different analytical techniques are adopted to acquire some insight into the evaluation of the laser cleaning effect. The amount of paint residue is analyzed by field emission scanning electron microscopy (FE-SEM), energy-dispersive spectroscopy (EDS), Fourier-transform infrared spectrum (FTIR), and photothermal conversion performance. Furthermore, the damage to the substrate surface is assessed utilizing an X-ray diffractometer (XRD) and

true color confocal microscope (TCCM). After laser cleaning, the nanostructures are created on the Al alloy surface. The formation of such nanostructures is analyzed in detail. Finally, the removal mechanism is preliminarily discussed.

2 Experimental section

2.1 Sample material preparation

In the technological design of re-spraying aircraft surface coating, the aircraft skin is usually coated with the paint as primer with a thickness of 20–40 μm . The primer is directly coated on the surface of the aircraft. We choose a paint layer with a thickness of 30 μm on the substrate surface for our research. The 2A12-T4 Al alloy (Shenzhen Hongwang Mould Co., Ltd) is cut into substrate samples with a dimension of 10 mm \times 10 mm \times 3 mm. The samples are polished through emery paper with 1500 mesh and sequentially washed with deionized water and acetone (Tianjin Sanjiang Co., Ltd) three times to remove impurities (Fig. 1a, b, d). Then, the paint mainly composed of epoxy resin (Xiamen Hawk New Material Technology Co., Ltd) is sprayed on the surface of Al alloy to obtain a paint layer with a thickness of 30 μm (Fig. 1c, e, f). The epoxy resin is composed of the epoxy emulsion and cationic curing agent. After that, the prepared samples are dried in the surrounding air and stored in an airtight bag for subsequent experiments. The composition of 2A12-T4 Al alloy is shown in Table 1.

2.2 Experimental setup

The schematic diagram of the laser cleaning system in the experiment is shown in Fig. 2a. The process of paint removal is directly carried out in an ambient atmosphere using a nanosecond pulsed width Nd:YAG laser (Institute of Semiconductors, Chinese Academy of Sciences) with an average maximum power of 600 W. The detailed experimental parameters are shown in Table 2.

The laser beam is moved using a one-dimensional galvanometric mirror scanning head and focused on sample surface using F-theta lenses. The distance between F-theta and the sample is adjusted to 15 cm. The laser beam transmission system is installed on the computer numerically controlled workstation. The scanning path of laser cleaning is z-shaped; to achieve a symmetrical overlap rate of spots, the light spots located in the direction of the X-scanning path are treated equivalent, as shown in Fig. 2b. The clamping angle (θ) between the light spot and the horizontal direction is 0.16° . Then, the equivalent spot width (d) is 0.99 mm. The overlap rates of X direction (η_x) and Y direction (η_y) are expressed by Formula (1) and Formula (2):

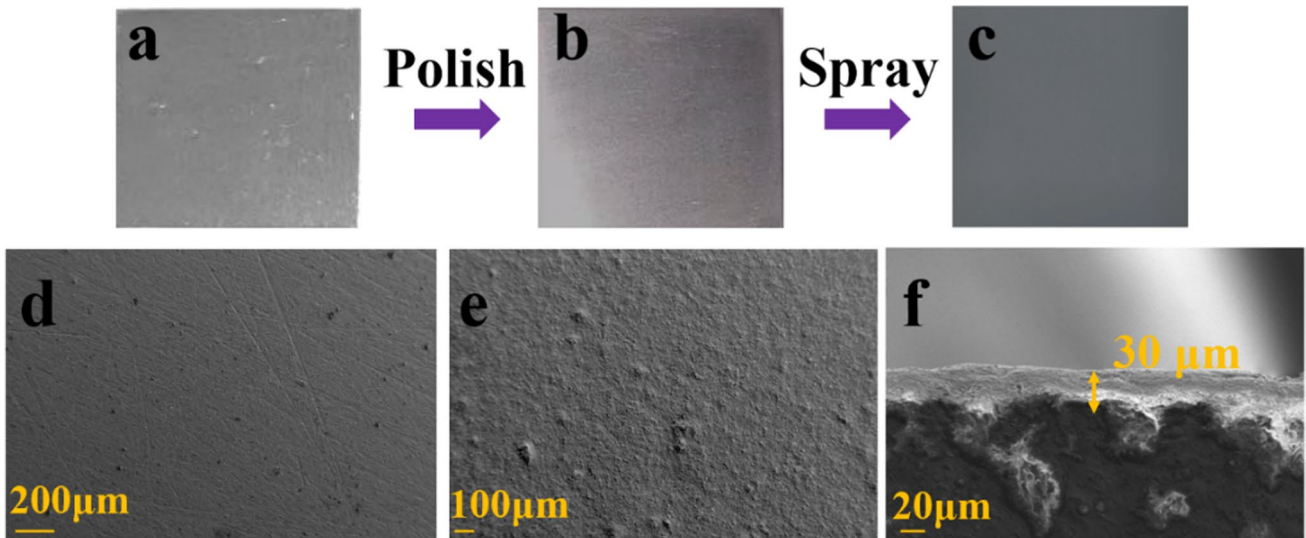
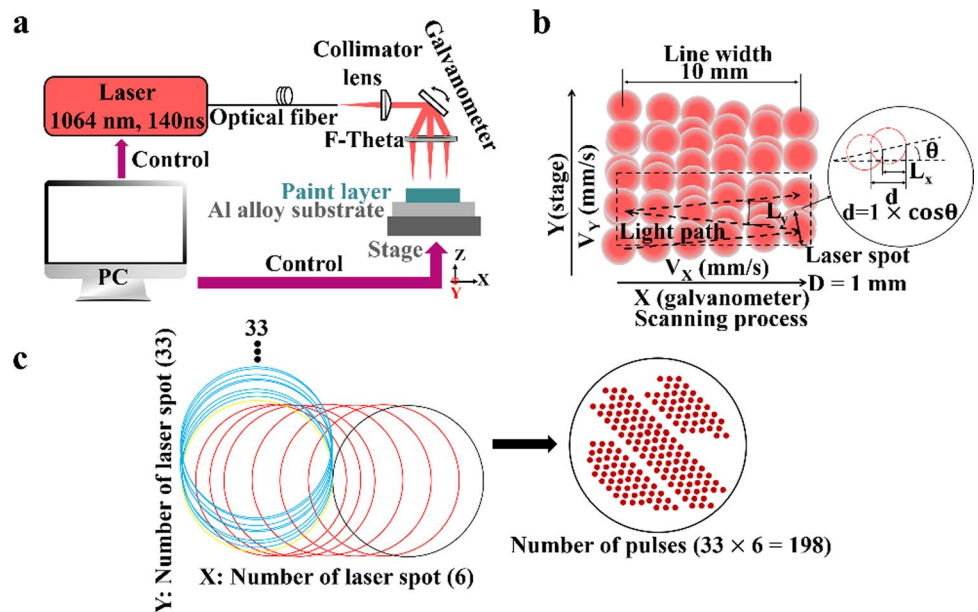


Fig. 1 Photographs of Al alloy (a), Al alloy after polishing (b), and Al alloy-paint (c) and SEM images of the surface of Al alloy after polishing (d), the surface of Al alloy-paint (e), and the cross-section of Al alloy-paint (f)

Table 1 Chemical composite of 2A12-T4 Al alloy

Elements	Al	C	Zn	O	Mg	Cu	Si	Cr	Mn
wt. %	78.24	9.43	5.50	2.18	2.01	1.28	0.97	0.20	0.19

Fig. 2 The schematic diagrams of the laser cleaning system (a), laser cleaning scanning path (b), and the number of pulses within a single laser spot (c)



$$\eta_x = 1 - \frac{V_x}{fd}$$

$$\eta_y = 1 - \frac{HV_y}{dV_x}$$

(1) According to Formulas (1) and (2), η_x and η_y are 84% and 97%, respectively. The effect of the overlap rates in the Y-direction must be taken into account when the number of pulses irradiated per spot can be calculated. Based on the point, the total number of pulses within a single laser spot is 198, as shown in Fig. 2c. The paint is scanned once

Table 2 Laser beam and scanning parameters

Parameter	Symbol	Value	Unit
Wavelength	λ	1064	nm
Outpower	P	60–320	W
Laser spot diameter	D	1	mm
Pulsed width	τ	140	ns
Pulsed frequency	f	20	kHz
Scanning speed (stage)	V_Y	6–16	mm/s
Galvanometer speed	V_X	3200	mm/s
Line width (galvanometer)	H	10	mm

in the scanning mode. The laser energy density can be calculated from Formula (3) [5, 21]:

$$F = \frac{4P}{f\pi D^2} \quad (3)$$

where F , P , f , and D are laser energy density, average output power, pulse frequency, and laser spot diameter, respectively.

2.3 Characterization

The surface morphology and elemental composition before and after laser cleaning are analyzed using a field emission scanning electron microscopy (FE-SEM; JEOL JMS-7500F, Japan) with an attached energy-dispersive spectroscopy (EDS). The metalloscope (DMM-480AC, China) is used to observe microscopic morphology. The surface roughness of the micro-areas ($328 \mu\text{m} \times 328 \mu\text{m}$) is detected using a true color confocal microscope (TCCM, CSM 700, Germany). The crystal structure is examined using a Bruker D8 Advance X-ray diffractometer (XRD) with Cu K α radiation ($k = 1.5418 \text{ \AA}$) in the 2θ range from 10 to 90° at 40 mA and 40 kV . Surface chemical composition is detected by Fourier-transform infrared spectrum (FTIR) spectrometer (Thermo Fisher Scientific, Nicolet iS50, America) with variable angle reflection attachment. The transparency and reflectance are recorded using a Shimadzu UV3600 spectrophotometer attached to an integrating sphere (ISR-3100). Atomic force microscopy (AFM) (Bruker, Dimension Icon) is used to analyze surface morphology. Thermogravimetric analysis (TG) is used to analyze the thermal decomposition behavior of paint. The paint is heated from 20 to $800 \text{ }^\circ\text{C}$ in the air and the speed of temperature increase is 10 K/min .

3 Results and discussion

To preliminarily observe the microscopic appearance evolution of laser irradiation areas, Fig. 3 presents the overall process window of laser irradiation areas as a function of

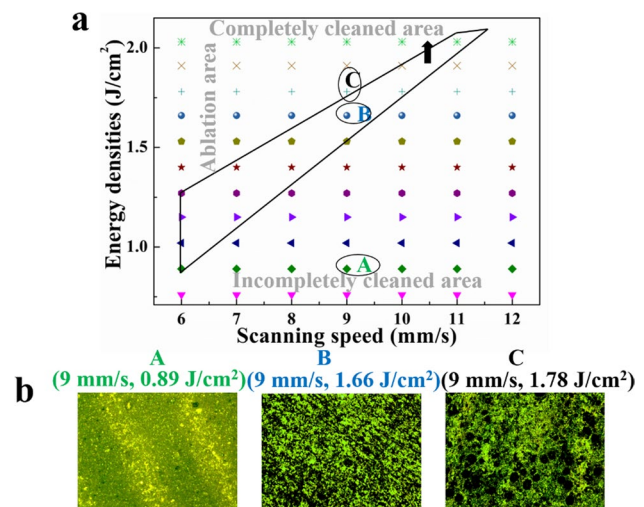


Fig. 3 (a) Process window—upper left: ablation area, middle: completely cleaned area, bottom right: incompletely cleaned area. (b) The micrograph images corresponding to A (9 mm/s , 0.89 J/cm^2), B (9 mm/s , 1.66 J/cm^2), and C (9 mm/s , 1.78 J/cm^2) from (a)

stage scanning speed (6 – 12 mm/s) and laser energy density (0.765 – 2.035 J/cm^2). According to microscopic morphology, the coordinate plane is divided into the incompletely cleaned area, the completely cleaned area, and the ablation area, as shown in Fig. 3a. It is seen that both laser energy density and stage scanning speed jointly determine the laser cleaning effect. In general, the lower the scanning speed, the lower the energy density required for complete cleaning. Selecting appropriate parameters enables the surface to reach a preferable cleaning effect. Considering the cleaning effect and cleaning efficiency, we investigate the effect of the energy densities range of 0.89 – 1.78 J/cm^2 on the removal of paint under the scanning speed of 9 mm/s . Figure 3b shows the micrograph images of laser irradiation areas (A, B, and C). With the laser condition of 0.89 J/cm^2 and 9 mm/s (A), the paint is unable to be completely removed. In the case of the laser energy density of 1.66 J/cm^2 and stage scanning speed of 9 mm/s (B), the paint is completely removed. For the laser energy density of 1.78 J/cm^2 and stage scanning speed of 9 mm/s (C), the ablation phenomenon begins to appear in the ablation area.

Figure 4 shows SEM images of Al alloy, Al alloy-paint, and laser cleaned paint. It is seen from Fig. 4a that there are some distinct scratches on the surface of Al alloy. After spraying paint, the surface is flat and pyknotic, indicating the formation of a certain thickness paint layer (Fig. 4b). The surface morphologies of laser cleaned paint with different energy densities are shown in Fig. 4c–i. As the energy density increases, the surface of laser cleaned paint gets rough. Also, the surface of Al alloy substrate is gradually exposed and forming a discontinued residuum on the surface of Al alloy, as shown in Fig. 4c–h. At a laser energy

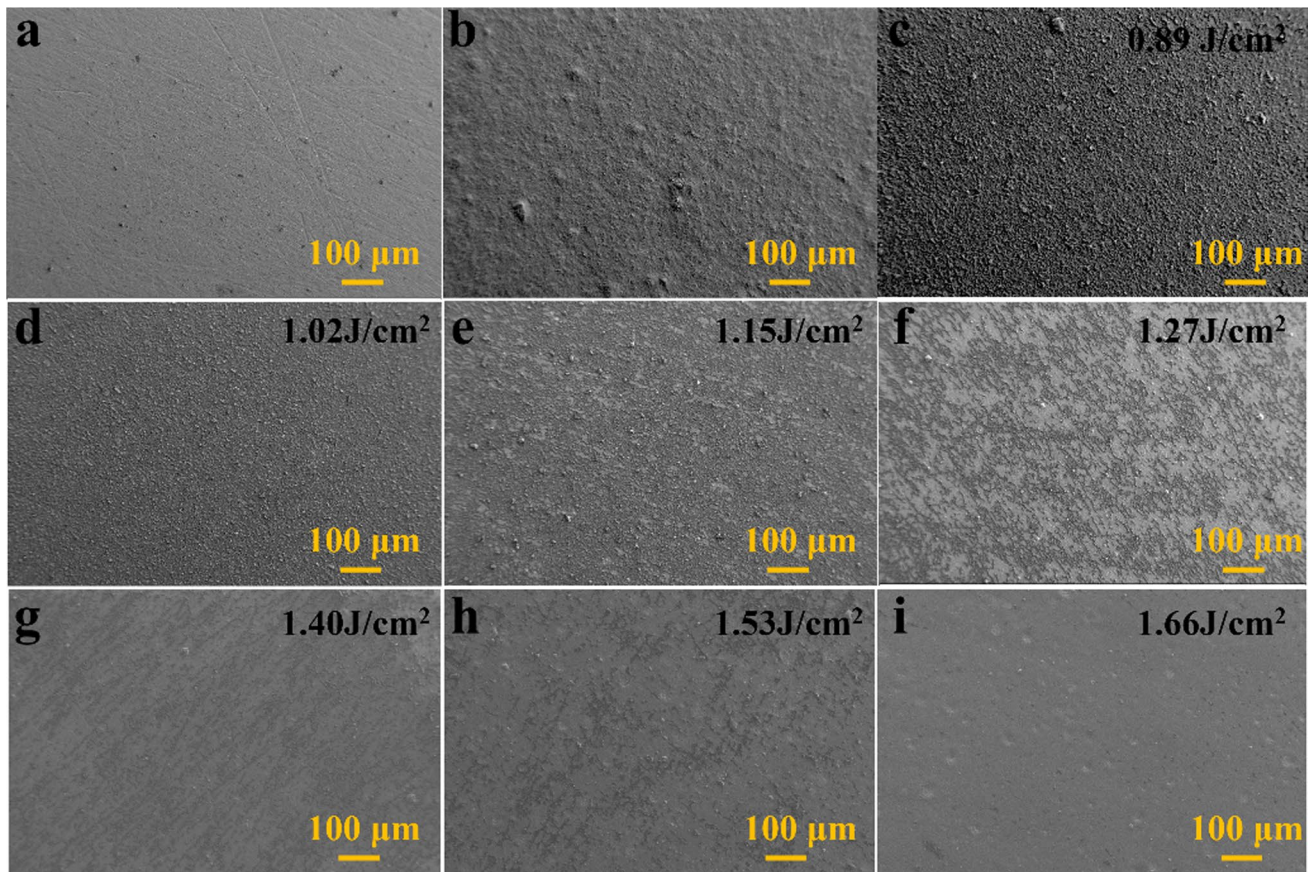


Fig. 4 SEM images of (a) Al alloy, (b) Al alloy-paint, and (c–i) laser cleaned paint at different energy densities: 0.89–1.66 J/cm²

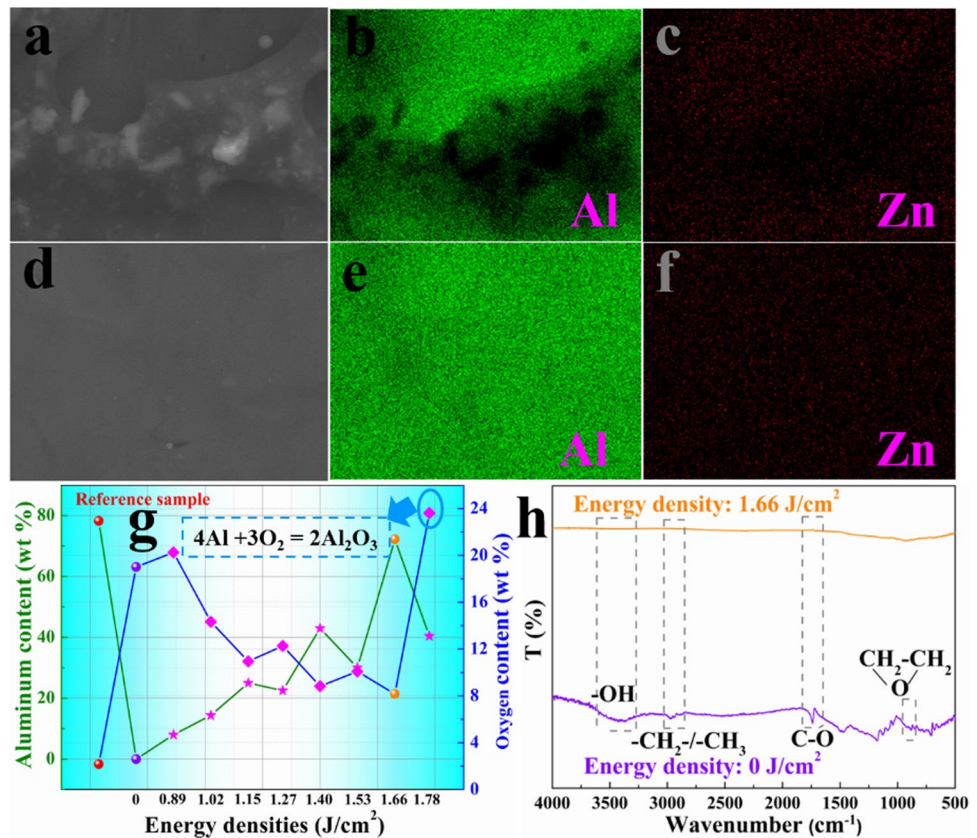
density is 1.66 J/cm², the whole Al alloy surface is observed (Fig. 4i). The result indicates that the paint layer is completely removed, while some obvious craters appear on the surface of Al alloy. It is likely to be due to the recoil pressure generated by the vaporization of the heated paint.

The laser irradiating the paint layer on the surface of Al alloy in the air is a complex process. To compare the laser cleaning effect, mapping images as an intuitional way play a crucial role in the analysis of element distribution. Due to the existence of abundant Al element and low content of Zn element in the Al alloy matrix, it is suitable for laser cleaned surface to detect the distribution of elements (Al and Zn). Figure 5a is the SEM image of the laser cleaned surface at the energy density of 1.53 J/cm². The distribution of Al and Zn elements mainly concentrates on the Al alloy surface, while partial regions display obvious shadows arising from the existence of paint residues, as shown in Fig. 5b and c. Figure 5d is the SEM image of the laser cleaned surface with an energy density of 1.66 J/cm². It is seen that Al and Zn elements are uniformly distributed on the laser cleaned surface (Fig. 5e, f). This indicates the inexistence of paint residues and a clean surface on the surface of Al alloy. Figure 5g shows the variation trend of mass percentage of Al

and oxygen before and after laser cleaning. The original Al alloy surface (reference sample) mainly consists of Al (~78 wt.%). After spraying paint, the Al content for Al alloy-paint is zero. With the increase of laser energy density in the range of 0.89–1.66 J/cm², Al content presents an upward tendency, and oxygen content decreases. This implies that the paint is gradually removed and the Al alloy substrate is exposed. It can be seen that the Al content of the laser cleaned surface with the energy density of 1.66 J/cm² reaches up to 72 wt.%, which is near that of the original Al alloy surface. This proves that the paint on the surface of Al alloy is completely removed at the energy density of 1.66 J/cm². However, with the energy density of 1.78 J/cm², Al content decreases, and the content of oxygen increases. It is deduced that the laser energy makes the surface temperature of Al alloy rise and causes Al alloy to melt [22].

Figure 5h shows the FT-IR spectra of Al alloy-paint and laser cleaned paint with the laser energy density of 1.66 J/cm². The FTIR spectra of Al alloy-paint exhibit the bands at 3406, 2975, 1741, and 884 cm⁻¹, which are the characteristic peaks for O–H stretching vibration, C–H stretching vibration, C–O stretching vibration, and epoxy group symmetric stretching vibration, respectively [23, 24]. For the

Fig. 5 SEM and mapping images with laser energy densities of 1.53 J/cm^2 (a–c) and 1.66 J/cm^2 (d–f). Diagram of element contents (g) and FT-IR spectra (h)



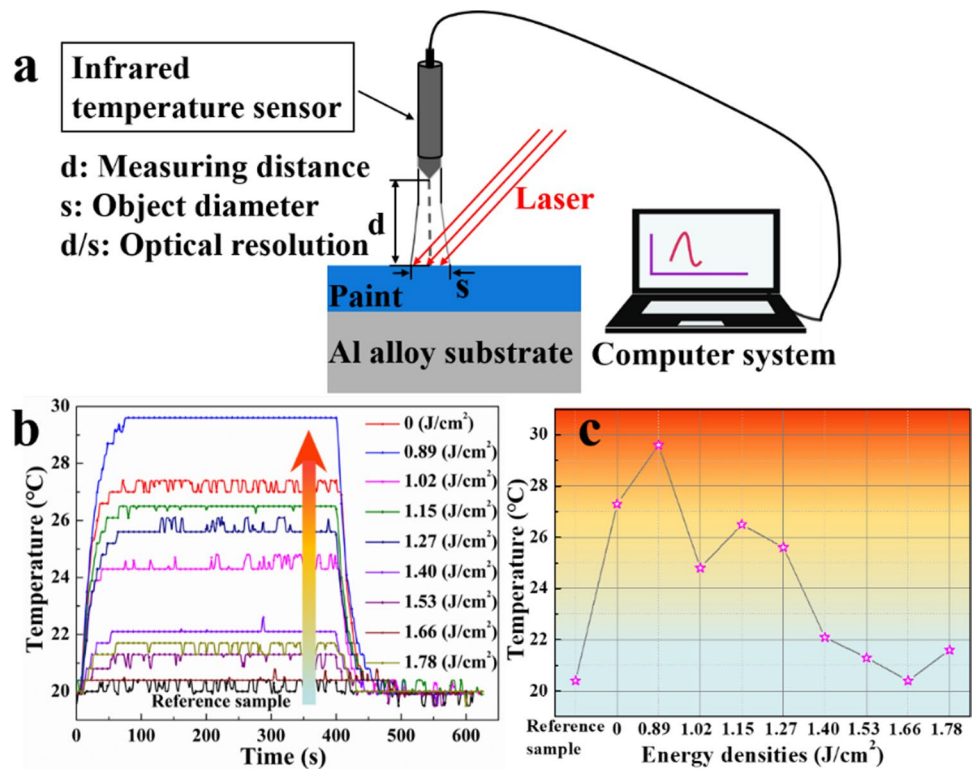
laser cleaned surface with the energy density of 1.66 J/cm^2 , these characteristic peaks disappear and get smooth owing to the thermal splitting of intricate functional group chains in the process of laser cleaning [25], which manifests a clean Al alloy surface.

To meet the cleaning effect requirements in the actual application, photothermal detection as a feasible non-destructive measurement technology is put forward to assess the amount of paint residue on Al alloy surface. It is easy to operate, convenient carrying, and suitable for large equipment. Figure 6a shows the schematic diagram of the measurement method. An 808-nm laser with a spot size of 25 mm^2 is used to directly irradiate the surface of samples. To observe apparent temperature change in the process of laser irradiation, laser power is adjusted to 1 W. The temperature is recorded by a temperature sensor with an accuracy of $\pm 0.1 \text{ }^\circ\text{C}$ tilted 45° relative to the path of the laser beam. An infrared temperature sensor is used to measure the temperature response of the laser irradiation area. The object diameter (s) is 10 mm, according to optical resolution (d/s , 20:1), and the measuring distance (d) is 200 mm. Figure 6b shows the relationship between the temperature as a function of laser irradiation time with data measured every second. The temperature responses of Al alloy-paint and laser cleaned surface with the energy densities of 0.89 – 1.27 J/cm^2 rapidly increase in the range

from 0 to 30 s, and the temperatures corresponded equilibrium states are 27.3 , 29.6 , 24.8 , 26.5 , and $25.6 \text{ }^\circ\text{C}$, respectively. The temperatures corresponded equilibrium state of Al alloy and laser cleaned surface with energy densities of 1.40 – 1.78 J/cm^2 are 20.4 , 22.1 , 21.3 , 20.4 , and $21.6 \text{ }^\circ\text{C}$, respectively. Despite appearing certain temperature fluctuations in the process of laser irradiation, the fluctuation range is negligible ($\pm 0.5 \text{ }^\circ\text{C}$).

The results indicate that temperature response might be concerned with paint thickness and surface structures (Fig. 4). It is seen from Fig. 6c that laser cleaned surface with the energy density of 0.89 J/cm^2 has a better photothermal conversion ability than Al alloy-paint owing to strong light absorption. With the increase of laser energy density, the equilibrium temperature of the laser cleaned surface decreases gradually. The result is primarily because the continuous vaporization of paint by thermal decomposition enables the thickness of paint to become thinner. When laser energy density is 1.66 J/cm^2 , the equilibrium temperature of the laser cleaned surface is the same as Al alloy, which indicates that the paint is completely removed. After laser irradiation (laser energy density: 1.78 J/cm^2), the equilibrium temperature of the laser cleaned surface has visibly turned up. This means that the laser energy density not only removes paint but also affects the substrate surface. The conclusion agrees with the former characterization results.

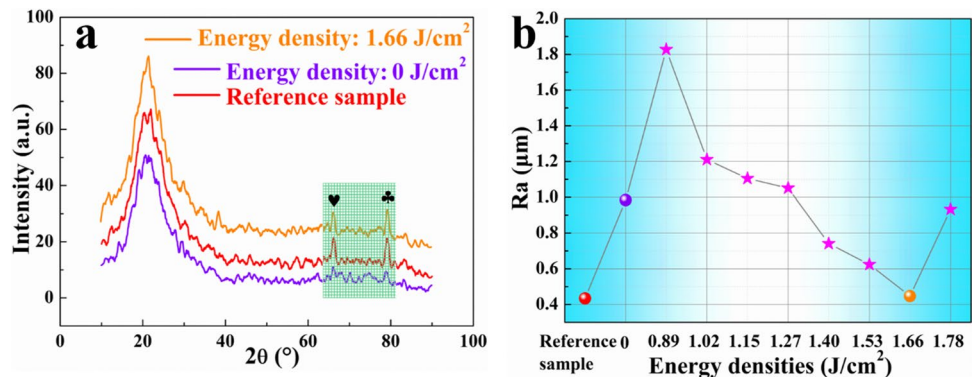
Fig. 6 (a) Schematic diagram of the measurement method. (b) The photothermal temperature curves and equilibrium temperature (c) of Al alloy, Al alloy-paint, and laser cleaned surface



Apart from paint residue on the surface of Al alloy substrate considerations, the extent of substrate surface damage is also an important aspect for the evaluation of the laser cleaning effect. The effect of the surface quality of material on geometric features and physical properties is crucial for further application. XRD analysis phase characteristics of Al alloy, Al alloy-paint, and laser cleaned surface are shown in Fig. 7a. It is observed for Al alloy-paint that no obvious diffraction peaks are detected, which further indicates that paint on the surface of Al alloy has a certain thickness. For Al alloy, the diffraction peaks corresponding to (220) and (311) planes of α -Al phase are observed. After laser cleaning of paint with the energy density of 1.66 J/cm², the diffraction peak intensity of laser cleaned surface is the same as Al alloy. The α -Al phase hardly is changed by the laser

energy density. To uncover micro-topographical changes of laser cleaned surface, the surface roughness of the micro-areas on the laser cleaned surface as a function of different laser energy density is shown in Fig. 7b. When laser energy density is 0.89 J/cm², the surface roughness of laser cleaned surface directly rises to 1.82 μm . With the consideration of the preceding analysis results from SEM and EDS, the arisen reason is attributed to the formation of irregular structure owing to the melted paint surface and solidification again in the laser cleaned area. With the increase of laser energy densities ranging from 1.02 to 1.53 J/cm², the surface roughness of laser cleaned surfaces declines slowly. At the energy density of 1.66 J/cm², the surface roughness of the laser cleaned surface is close to Al alloy, which indicates that the paint layer is completely removed. When laser energy

Fig. 7 XRD results (a) and the surface roughness (b)



density reaches 1.78 J/cm^2 , the surface roughness of the Al alloy substrate increases again which is likely to be associated with the newly generated structures.

The mechanisms of pulsed laser cleaning of paint in the previous literature include ablation and vibration. In the present experiment as shown in Fig. 8a, at 1064 nm, the absorptivity of paint is about 91%, and the transmittance is very small. According to Beer–Lambert law, the absorption coefficient of paint can be 200/mm. Therefore, the paint can be regarded as opaque at 1064 nm wavelength. The ablation process is mainly considered. The TG as an effective thermo-analysis technology is used to research the relationship between physical characteristics and temperature, as shown in Fig. 8b. The results show that the paint begins to melt at 171 °C, and thermal decomposition temperature is 370 °C.

Combined with the above analysis, it is essential to consider the model based on laser energy distribution in the thickness direction of paint for the understanding of the mechanism, as shown in Fig. 9a. The model geometry consists of a 30- μm -thick paint film on the surface of Al alloy substrate. The following assumptions are met in the model:

1. The heat transfer in the form of convection, heat conduction, and thermal conduction is ignored.
2. The distribution of laser energy is homogeneous, only considering the temperature change of the paint.

As noted in Fig. 9a, the energy absorbed (dE) by the paint with thickness dz at the depth of z_t is shown in Formula (4) based on Beer–Lambert law, where E_1 , E_2 , and E_L are the incident laser energy of the paint layer, the transmission laser energy of the paint layer, and the laser pulse energy, respectively. R and α indicate the reflectivity and the laser absorption coefficients of paint. The detailed equations are expressed as follows:

$$dE = E_1 - E_2 = (1 - R)E_L e^{-\alpha z_t} - (1 - R)E_L e^{-\alpha(z_t+dz)} \quad (4)$$

After absorbing laser energy, paint experiences phase change states, which are solid, liquid, and vapor, respectively.

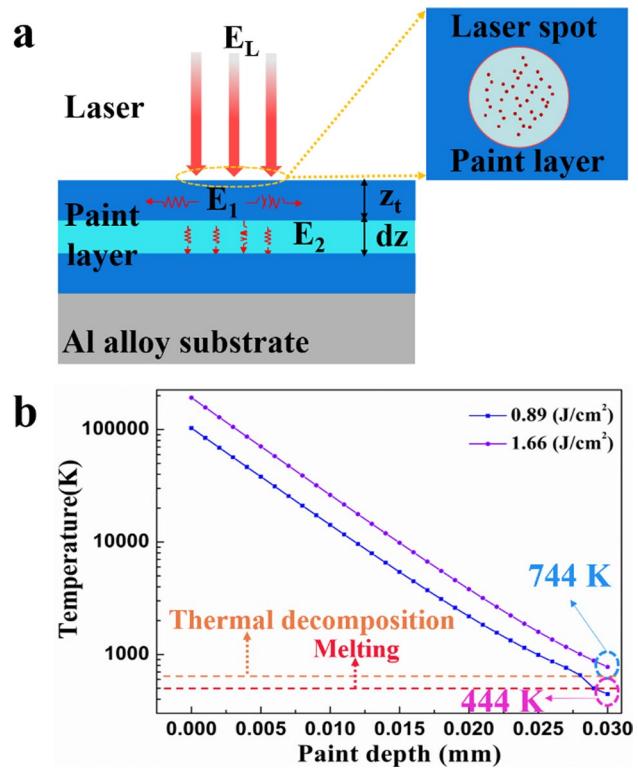


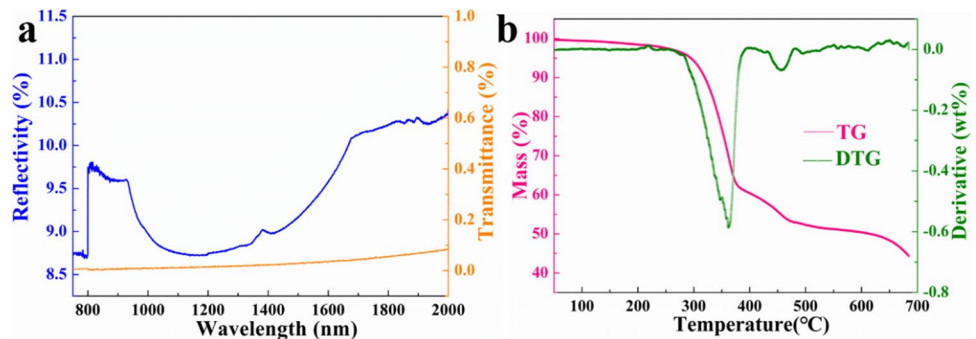
Fig. 9 (a) Diagram of laser energy distribution model. (b) The temperature of the paint varies with the paint depth

With the consideration of the effect of laser spot overlap rates, the total number of pulses irradiated on per unit area of the paint surface is 198. According to the relationship between the temperature and energy [26], the temperature can be deduced under different conditions:

$$T_2 = \frac{198(1 - R)(1 - e^{-\alpha dz})e^{-\alpha z_t} FM}{c\rho dz} + T_1 \quad (5)$$

$$T_2 = \frac{198(1 - R)(1 - e^{-\alpha dz})e^{-\alpha z_t} FM}{c\rho dz} - \frac{\Delta H_M}{c} + T_1 \quad (6)$$

Fig. 8 (a) The reflectance and transmission spectra and (b) TG-DTG result of paint



$$T_2 = \frac{198(1 - R)(1 - e^{-\alpha z})e^{-\alpha z}FM}{\rho dz} - \frac{\Delta H_M}{c} - \frac{\Delta H_V}{c} + T_1 \tag{7}$$

where T_1 , T_2 , ρ , and c indicate the initial temperature, final temperature, density, and heat capacity. F and M stand for laser energy density and molar mass. ΔH_M and ΔH_V indicate molar enthalpy of fusion and molar enthalpy of vaporization.

By substituting the physical parameters of paint in Table 3, the relationship between paint temperature and paint depth can be obtained, and the result is shown in Fig. 9b. When laser energy density is 0.89 J/cm², the temperature at the depth of 28 μm is 653 K, which has reached the thermal decomposition temperature of paint. The remanent paint on the laser cleaned surface can appear as fusion, which agrees with the result in Fig. 4c. At 1.66 J/cm², the temperature at the depth of 30 μm is 774 K, which reaches the thermal decomposition temperature. For the Al alloy substrate, the melting point is 933 K. Therefore, with the laser energy density of 1.66 J/cm², the 30 μm of paint can be completely removed through instantaneous decomposition gasifying, which is consistent with the result of SEM (Fig. 4i). From the above result observation, because of the strong absorption capacity of paint in 1064 nm wavelength, local high heat generated (the thermal diffusivity, $\vartheta = k/\rho c$, $2.47 \times 10^{-7} \text{ m}^2\text{s}^{-1}$) on the surface layer of paint results in the rise in temperature. When the paint temperature reaches the thermal decomposition temperature, the paint is vaporized and removed. With the increase of laser energy densities, the thickness of paint on the surface of Al alloy gradually decreases. Within a certain laser energy density control range, the paint can be completely removed, however, Al alloy substrate still maintains intrinsic thermodynamic properties owing to the high melting point.

In addition, basing on the above analysis, when a laser energy density is 1.78 J/cm², the surface characteristics of Al alloy experience some changes. It is essential to discuss the case. Figure 10a shows the SEM image of the laser cleaned paint at laser energy densities of 1.78 J/cm². The paint is not

only completely removed but the newly formed cracks also appear on the surface of Al alloy. These cracks propagate along the different directions. In order to clearly observe the structures marked by the red circle in Fig. 10a, AFM with nanometer resolution is applied to analyze the morphology. The cracks at two locations are selected in the AFM image, as shown in Fig. 10b. The sectional line at location 1 shows that the depth of the cracks is about 100 nm (Fig. 10c). Location 2 also presents similar results. The results indicate that the nanostructures with a V-shape are generated on the surface of the Al alloy. The surface temperature calculation is conducted based on the model from Fig. 9a. Figure 10d shows that the temperature on the surface of Al alloy at the paint depth of 30 μm is 935.8 K, which is higher than the melting temperature of Al alloy (933 K). It means that the surface of Al alloy experiences the melting state, as shown in Fig. 10e. The chemical bonds (Al–Al) in the melting state rapidly break due to the thermal fluctuation. In this stage, the atomic repulsion can be generated, which is conducive to crack formation [31]. Furthermore, surface tension has a direct relationship with temperature. When the surface of the melting layer is not at a uniform temperature, the surface tension has a remarkable difference. When the surface temperature in the melting layer decreases, the surface tension will increase [32, 33]. Because the laser energy for laser paint stripping is in a Gaussian distribution, and with the superposition of multiple pulses, temperature gradients on the surface of the melting layer can be developed. The liquid in the high-temperature region on the surface of the melting layer is pulled to the low-temperature region due to the difference of surface tension, as shown in Fig. 10f. With decreasing temperature, the number of covalent bonds gradually increases, and the melting material will be solidified. The V-shape nanostructures on Al alloy surface can be ascribed to action of high-energy laser. These nanostructures may give the surface with new physical properties, such as the anti-reflection, corrosion resistance, and hydrophobic ability [34–36].

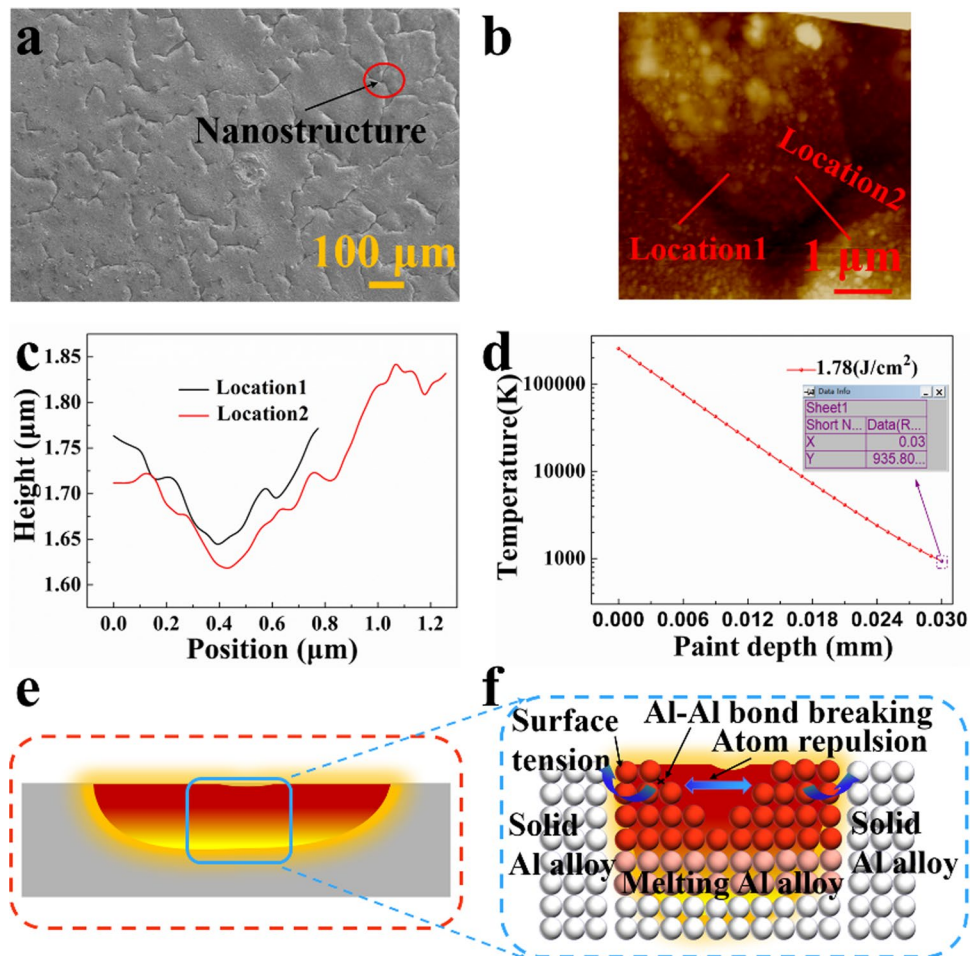
4 Conclusions

In this study, the effect of different laser energy densities on the removal of paint on the surface of Al alloy is investigated by an environment-friendly nanosecond pulsed laser. Different analytical techniques (FE-SEM, EDS, FTIR, photothermal conversion performance, XRD, and TCCM) are adopted to evaluate the laser cleaning effect. Key laser energy nodes are given; one is the critical point for effective paint removal, and the other is the critical point for the morphology change of the substrate surface. As laser energy density increases, the removal thickness of paint gradually increases. With the laser energy density of

Table 3 Physical parameters of paint

Physical parameters	Paint
Density (ρ , g/mm ³)	1.2×10^3
Reflectivity (R)	8.7%
Absorption coefficient (α , /mm)	200
Molar heat capacity (c , J/(mol·K))	379 [27, 28]
Molar mass (M , g/mol)	151 [26]
Molar enthalpy of fusion (ΔH_M , J/mol)	14,560 [29]
Molar enthalpy of vaporization (ΔH_V , J/mol)	62,300 [30]
Melting point (K)	444
Thermal decomposition temperature (K)	744

Fig. 10 (a) The SEM image with laser energy density of 1.78 J/cm^2 . (b) The AFM image of the structures marked by the red circle in (a). (c) The image of the section lines of location 1 and location 2 marked by the red lines in (b). (d) The temperature of the paint varies with the paint depth. (e, f) Schematic of nanostructures formation mechanism on the surface of Al alloy



1.66 J/cm^2 , the cleaning effect can reach the best. Al content and the roughness are close to those of the original Al alloy surface. Some characteristic peaks of paint disappear in the FT-IR spectra. The relationship between temperature and energy shows that the mechanism of paint removal is mainly the thermal decomposition. When laser energy density increases to 1.78 J/cm^2 , the surface of Al alloy forms some nanostructures. The laser cleaning technology can achieve an excellent effect in paint removal to form a new surface morphology with such physical properties as the corrosion resistance, anti-reflection, and hydrophobic ability.

Author contribution FS: conceiving the idea; FS and ZZ: data analysis and writing—original draft; ZZ, LL, ZC, YT, MC, and XL: investigation, experimental, characterization, methodology; ZZ: simulating computation.

Funding This work is supported by the National Key Research and Development Program of China (Grant No. 2022YFB4601500), National Key R&D Plan (Grant No. 2021YFB3502701), and National Natural Science Foundation of China (NSFC) (Grant No.12174206).

Availability of data and materials The authors guarantee no restriction of availability of data and material.

Declarations

Human and animal rights and informed consent This article does not contain any studies with human participants or animals performed by any of the authors.

Conflict of interest The authors declare no competing interests.

References

- Ding YM, Liu SG, Xia CQ, Zou XR, Liu D, Wang YQ, Yang T, Li Q (2021) Thermal oxidation of novel Zr-Ti-Al-V alloy with high strength and toughness and its influence on the corrosion behavior. *Surf Coat Technol* 423(10):127576
- Syaifudin A, Nurfadillah EM, Farid AR, Windharto A (2021) Strength consideration on car body of light rail transit making from aluminum extrusion. *IOP Conf Ser Mater Sci Eng* 1034(1):012025

3. Hirsch J (2014) Recent development in aluminum for automotive applications. *Trans Nonferrous Metals Soc China* 24(7):1995–2002
4. Li YJ, Yu SF, Chen Y, Yu RZ, Shi YS (2020) Wire and arc additive manufacturing of aluminum alloy lattice structure. *J Manuf Process* 50:510–519
5. Shan T, Yin FS, Wang SJ, Qiao YL, Liu P (2020) Surface integrity control of laser cleaning of an aluminum alloy surface paint layer. *Appl Opt* 59(30):9313–9319
6. Chen GX, Kwee TJ, Tan KP, Choo YS, Hong MH (2010) Laser cleaning of steel for paint removal. *Appl Phys A-Mater Sci Process* 101(2):249–253
7. Gotoh K, Harayama K, Handa K (2015) Combination effect of ultrasound and shake as a mechanical action for textile cleaning. *Ultrason Sonochem* 22:412–421
8. Mainord K (2001) Reducing solvent and chemical cleaning of laboratory glassware. *Am Lab* 33(17):24–27
9. Zhang BC, Jia XJ, Li FY, Sun YH (2019) Research on the effect of molten salt ultrasonic composite cleaning for paint removal. *ACS Omega* 4(16):17072–17082
10. Carvalho L, Pacquentin W, Tabarant M, Semerok A, Maskrot H (2020) Metal decontamination by high repetition rate nanosecond fiber laser: application to oxidized and Eu-contaminated stainless steel. *Appl Surf Sci* 526:146654
11. Zuo JX, Lin XC (2022) High-power laser systems. *Laser Photon Rev* 16(5):2270025
12. Tsunemi A, Hagiwara K, Saito N, Nagasaka K, Miyamoto Y, Suto O, Tashiro H (1996) Complete removal of paint from metal surface by ablation with a TEA CO₂ laser. *Appl Phys A-Mater Sci Process* 63:435–439
13. Lu Y, Ding Y, Wang ML, Yang LJ, Wang Y (2021) A characterization of laser cleaning painting layer from steel surface based on thermodynamic model. *Int J Adv Manuf Technol* 116(5–6):1989–2002
14. Reitz V, Meinhard D, Ruck S, Riegel H, Knoblauch V (2017) A comparison of IR- and UV-laser pretreatment to increase the bonding strength of adhesively joined aluminum/CFRP components. *Compos A Appl Sci Manuf* 96:18–27
15. Miao RP, Wang T, Yao T, Hu SW, Huang XD, Kang QC (2021) Experimental and numerical simulation analysis of laser paint removal of aluminum alloy. *J Laser Appl* 34(1):012002
16. Zhou X, Imasaki K, Furukawa H, Umino H, Sakagishi K, Nakai S, Yamanaka C (2001) Simulation study and experiment on laser-ablation surface cleaning. *Opt Laser Technol* 33(3):189–194
17. Shi SD, Li W, Du P, Wang M, Song F, Liu SJ, Chen NJ, Zhao H, Yang WJ (2012) Removing paint from a metal substrate using a flattened top laser. *Chin Phys B* 21(10):104209
18. Han JH, Cui XD, Wang S, Feng GY, Deng GL, Hu RF (2017) Laser effects based optimal laser parameter identifications for paint removal from metal substrate at 1064nm: a multi-pulse model. *J Mod Opt* 64(19):1947–1959
19. Lu Y, Yang LJ, Wang ML, Wang YW (2020) Improved thermal stress model and its application in ultraviolet nanosecond laser cleaning of paint. *Appl Opt* 59(25):7652–7659
20. Zhao HC, Qiao YL, Zhang Q, Du X, Han BY (2020) Study on the characteristics and mechanism of pulsed laser cleaning of polyacrylate resin coating on aluminum alloy substrates. *Appl Opt* 59(23):7053–7065
21. Zhang GX, Hua XM, Huang Y, Zhang YL, Li F, Shen C, Cheng J (2020) Investigation on mechanism of oxide removal and plasma behavior during laser cleaning on aluminum alloy. *Appl Surf Sci* 506:144666
22. Zhu GD, Wang SR, Cheng W, Wang GQ, Liu WT, Ren Y (2019) Investigation on the surface properties of 5A12 aluminum alloy after Nd: YAG laser cleaning. *Coatings* 9(9):578
23. Xu HY, Lu D, Han X (2020) Graphene-induced enhanced anti-corrosion performance of waterborne epoxy resin coating. *Front Mater Sci* 14(2):211–220
24. Meure S, Wu DY, Furman SA (2010) FTIR study of bonding between a thermoplastic healing agent and a mendable epoxy resin. *Vib Spectrosc* 52(1):10–15
25. Zhao HC, Qiao YL, Du X, Wang SJ, Zhang Q, Zang Y, Cai ZH (2019) Paint removal with pulsed laser: theory simulation and mechanism analysis. *Appl Sci Basel* 9(24):5500
26. Zhang DH, Xu J, Li ZC, Jin Y, Su X, Shan DB, Guo B (2022) Removal mechanisms of nanosecond pulsed laser cleaning of blue and red polyurethane paint. *Appl Phys A* 128(2):170
27. Lu Y, Yang LH, Wang Y, Chen H, Guo B, Tian Z (2019) Paint removal on the 5A06 aluminum alloy using a continuous wave fiber laser. *Coatings* 9(8):488
28. Li XK, Zhang QH, Zhou XZ, Zhu DQ, Liu QX (2017) The influence of nano-second laser pulse energy density for paint removal. *Optik* 156:841–846
29. Chickos JS, Acree WE, Liebman JF (1999) Estimating solid-liquid phase change enthalpies and entropies. *J Phys Chem Ref Data* 28(6):1535–1673
30. Chickos JS (2003) Enthalpies of vaporization of organic and organo-metallic compounds. *J Phys Chem Ref Data* 32(2):519–878
31. Lin ZY, Ji LF, Hong MH (2022) Approximately 30 nm nanogroove formation on single crystalline silicon surface under pulsed nanosecond laser irradiation. *Nano Lett* 22(17):7005–7010
32. Pearson JRA (1958) On convection cells induced by surface tension. *J Fluid Mech* 4(5):489
33. Xu JM, Chen MM, Liu ZQ, Wang J, Liu LM, Han ZC, Xu HB (2019) Investigation of wavelength effects on polycrystalline silicon damages using nanosecond pulse laser irradiation. *J Mater Process Technol* 267:159–166
34. Yong JL, Chen F, Qing Y, Farooq U, Hou X (2015) Photoinduced switchable underwater superoleophobicity-superoleophilicity on laser modified titanium surfaces. *J Mater Chem A* 3(20):10703–10709
35. Pan AF, Wang WJ, Mei XS, Zheng BX, Yan ZX (2016) Cracks growth behaviors of commercial pure titanium under nanosecond laser irradiation for formation of nanostructure-covered microstructures (with sub-5- μ m). *Appl Surf Sci* 387:1046–1053
36. Dobrzanski LA, Drygala A, Golombek K, Panek P, Bielanska E, Zieba R (2008) Laser surface treatment of multicrystalline silicon for enhancing optical properties. *J Mater Process Technol* 201(1–3):291–296

Publisher's note Springer Nature remains neutral with regard to jurisdictional claims in published maps and institutional affiliations.

Springer Nature or its licensor (e.g. a society or other partner) holds exclusive rights to this article under a publishing agreement with the author(s) or other rightsholder(s); author self-archiving of the accepted manuscript version of this article is solely governed by the terms of such publishing agreement and applicable law.